Accelerated Proton Echo Planar Spectroscopic Imaging (PEPSI) Using GRAPPA with a 32-Channel Phased-Array Coil

Shang-Yueh Tsai,[1] Ricardo Otazo,[2] Stefan Posse,[2,3] Yi-Ru Lin,[4] Hsiao-Wen Chung,[1] Lawrence L. Wald,[5] Graham C. Wiggins,[5] and Fa-Hsuan Lin[5–7*]

Parallel imaging has been demonstrated to reduce the encoding time of MR spectroscopic imaging (MRSI). Here we investigate up to 5-fold acceleration of 2D proton echo planar spectroscopic imaging (PEPSI) at 3T using generalized autocalibrating partial parallel acquisition (GRAPPA) with a 32-channel coil array, 1.5 cm^3 voxel size, TR/TE of 15/2000 ms, and 2.1 Hz spectral resolution. Compared to an 8-channel array, the smaller RF coil elements in this 32-channel array provided a 3.1-fold and 2.8-fold increase in signal-to-noise ratio (SNR) in the peripheral region and the central region, respectively, and more spatial modulated information. Comparison of sensitivity-encoding (SENSE) and GRAPPA reconstruction using an 8-channel array showed that both methods yielded similar quantitative metabolite measures ($P > 0.1$). Concentration values of *N*-acetyl-aspartate (NAA), total creatine (tCr), choline (Cho), myo-inositol (mI), and the sum of glutamate and glutamine (Glx) for both methods were consistent with previous studies. Using the 32-channel array coil the mean Cramer–Rao lower bounds (CRLB) were less than 8% for NAA, tCr, and Cho and less than 15% for mI and Glx at 2-fold acceleration. At 4-fold acceleration the mean CRLB for NAA, tCr, and Cho was less than 11%. In conclusion, the use of a 32-channel coil array and GRAPPA reconstruction can significantly reduce the measurement time for mapping brain metabolites. Magn Reson Med 59:989–998, 2008. © 2008 Wiley-Liss, Inc.

Key words: proton echo planar spectroscopic imaging; PEPSI; MR spectroscopic imaging; parallel MRI; 32-channel phase array; GRAPPA

MR spectroscopic imaging (MRSI) plays important roles in both clinical diagnosis and biomedical research. One of the main challenges of the conventional MRSI techniques is the lengthy data acquisition time, a result of the many phase-encoding steps required for complete spatial encoding. Several methods have been proposed to reduce scanning time using reduced or weighted *k*-space acquisition (1). Other methods acquire multiple (typically two to four) individually phase-encoded spin echoes within a single RF excitation to reduce encoding time (2). However, because the acquisition of multiple echoes requires shortened echo spacing, such a method is characterized by a limited spectral resolution. Alternatively, it is possible to acquire all the spatial information in a single shot using fast imaging readout modules, and to encode the spectral information by incrementing the spectral evolution time in separate RF excitations (3–6). In this way, spatial resolution is independent of scanning time, thus high spatial resolution can be achieved. However, the disadvantage of such approaches is the time-consuming spectral encoding process required to achieve high spectral resolution and bandwidth. Proton echo planar spectroscopic imaging (PEPSI) (7–9) uses an oscillating readout gradient to simultaneously acquire spatial and spectral information in a single RF excitation. PEPSI yields spectral resolution that approximates that of conventional MRSI and enables a reduction in the encoding time by a factor of more than an order of magnitude. PEPSI was developed for clinical MR scanners to measure 2D metabolite distributions in 1 min and 3D metabolite distributions in several minutes (10,11); the technique has been employed in clinical studies (12,13).

The development of parallel MRI techniques (14–17) has enabled a significant reduction in imaging time, as phase-encoding steps can be partially replaced by the spatial information inherent in a multiple-channel receiver coil array with nonuniform spatial sensitivities. Parallel MRI techniques can be used in combination with either standard MRSI (18,19) or fast MRSI (20) to reduce data acquisition time. We have recently demonstrated that the use of a combined PEPSI and a sensitivity-encoding (SENSE) technique with an 8-channel coil array achieves sub-minute MRSI data acquisition at the cost of reduced signal-to-noise ratio (SNR) (21). Two major factors limit the acceleration factor attainable for parallel MRI: the number of receiver channel coils and the SNR of the MR acquisitions. By using a coil array with a large number of channels, we may further improve the temporal resolution and the SNR of PEPSI in a parallel MRI strategy. The enhanced SNR made possible by an array of smaller RF coil elements enables tessellation of the cortical coverage,

[1]Department of Electrical Engineering, National Taiwan University, Taipei, Taiwan.

[2]Departments of Electrical & Computer Engineering, University of New Mexico, Albuquerque, New Mexico, USA.

[3]Department of Psychiatry, University of New Mexico School of Medicine, Albuquerque, New Mexico, USA.

[4]Department of Electronic Engineering, National Taiwan University of Science and Technology, Taipei, Taiwan.

[5]MGH-HMS-MIT Athinoula A. Martinos Center for Biomedical Imaging, Charlestown, Massachusetts, USA.

[6]Department of Radiology, Massachusetts General Hospital, Boston, Massachusetts, USA.

[7]Institute of Biomedical Engineering, National Taiwan University, Taipei, Taiwan.

Grant sponsor: National Institutes of Health; Grant numbers: R01 HD040712, R01 NS037462, R01 EB000790, P41 RR14075; Grant sponsor: Mental Illness and Neuroscience Discovery (MIND) Institute; Grant sponsor: Ministry of Education (international student exchange program to S.Y.T.).

*Correspondence to: Fa-Hsuan Lin, PhD, Athinoula A. Martinos Center for Biomedical Imaging, Bldg. 149, 13th St., Mail code 149-2301, Charlestown, MA, 02129. E-mail: fhlin@nmr.mgh.harvard.edu; Institute of Biomedical Engineering, National Taiwan University, 1, Sec. 4, Roosevelt Rd., 106 Taipei, Taiwan. E-mail: fhlin@ntu.edu.tw.

Received 9 February 2007; revised 9 November 2007; accepted 8 December 2007.

DOI 10.1002/mrm.21545
Published online in Wiley InterScience (www.interscience.wiley.com).

and the acquisition of more spatially disparate information from different channels in the array improves image reconstruction of parallel MRI. The further reduction in scan time reduces motion sensitivity and thus offers the potential benefit of reducing motion artifacts for patients who are incapable of remaining still for lengthy scans. PEPSI has been employed for time-resolved metabolic imaging to characterize metabolic dysfunction during sodium-lactate infusion in patients with panic disorder (12), and to detect the elevated lactate level in children during an auditory-based language task (22). Highly accelerated MRSI with better temporal resolution may also facilitate monitoring of a possible transient metabolic response to time-locked stimuli using multiple trials.

Recently, coil arrays have been designed with as many as 32 channels to accelerate structural and functional MRI (23–25), and the 32-channel array has been demonstrated to improve SNR by a factor of 3.5 in the lateral cortex and a factor of 1.5 in the corpus callosum when compared with an 8-channel head coil consisting of eight surface coils covering the entire head circumferentially (25). Additionally, the 32-channel array can reduce noise amplification (g-factor) by 1.5-fold in 1D parallel MRI at 4-fold acceleration (25).

To date, the most widespread parallel MRI techniques are the sensitivity encoding (SENSE), which works in the image domain, and the generalized partial parallel acquisition (GRAPPA), which works in *k*-space. Both methods can provide good results with nearly identical reconstruction quality, and they are available for clinical routine (26). We have demonstrated that SENSE can be applicable for PEPSI acceleration (21) and we chose GRAPPA reconstruction in this study because an explicit estimation of coil sensitivity profiles is not required.

Here we report the results of our in vivo experiments employing a 32-channel head coil array at 3T (25) to investigate the feasibility of accelerating data acquisition up to 5-fold along a single phase-encoding direction with the use of PEPSI and GRAPPA reconstruction (16). We also compared and evaluated the reconstruction performance of GRAPPA and SENSE using an 8-channel coil array. This comparison has not been performed yet for MRSI and presents differences to structural image reconstruction due to the low-resolution characteristics. The dominant cerebral metabolites, including singlets of *N*-acetyl-aspartate (NAA), total creatine (tCr), including creatine (Cr) and phosphocreatine (PCr), and choline (Cho), as well as complex multiplets of myo-inositol (mI) and the combination of glutamate and glutamine (Glx) were measured and quantified in accelerated MRSI experiments at 3T.

MATERIALS AND METHODS

Experiments

Experiments on both human subjects and a spectroscopy phantom were performed using a 3T scanner (Siemens MAGNETOM Trio, Siemens Medical Solutions, Erlangen, Germany) equipped with an 8-channel head coil array (Siemens Medical Solutions) that covers the entire head circumferentially with eight surface coils, and a 32-channel head coil array (25). The 32-channel array consists of small circular receiver coils overlapped to minimize the mutual inductance between neighboring coils. Two types of coil elements (8.5 cm and 6 cm diameters) were arranged evenly to wrap around the whole head on a close-fitting fiberglass helmet modeled after the European standard head norm EN960/1994 for protective headgear (25). The array is referred to as having a soccer ball geometry. In this study the discussion of the 32-channel coil array is specific to this coil geometry.

The PEPSI pulse sequence used in this study included water suppression by chemical shift selective saturation (CHESS) and a WET (water suppression enhanced through T_1 effects) technique; eight slices of outer volume lipid suppression were applied along the perimeter of the brain (Fig. 1), with spin-echo excitation and fast spatial-spectral encoding using an EPI readout gradient train along the X-axis. We acquired data at a bandwidth of 83.33 kHz, with 1024 gradient inversions and online regridding to account for gradient ramp sampling. Even-echo and odd-echo data were separately reconstructed as described previously (11). We applied a sinusoidal *k*-space filter to both nonwater-suppressed (NWS) and water-suppressed (WS) data to suppress side lobes of the point-spread function. The spectral width after even/odd echo editing was 1087 Hz, with 512 complex points. Phase encoding gradients were applied along the Y-axis to obtain 2D spatial encoding. In order to employ the GRAPPA technique for acceleration we reduced the phase encoding steps along the Y-axis by sampling one *k*-space line in a block of two, three, four, or five consecutive *k*-space lines, allowing us to achieve 2-, 3-, 4-, and 5-fold accelerations, respectively. We acquired both WS and NWS data; NWS data were collected without presaturation and were used for automatic phase and frequency shift corrections.

We acquired fully sampled and accelerated single-average in vivo PEPSI data from a para-axial slice at the upper edge of the ventricles using the following parameters: TR = 2 sec, TE = 15 ms, 32 × 32 spatial matrix, FOV = 240 mm, slice thickness = 15 mm, and voxel size = 0.85 cm^3 (Fig. 1). After application of the spatial sinusoidal filter, the voxel size was 1.9 cm^3. The data acquisition time was 64 sec for a fully sampled dataset; for the accelerated in vivo data with 2-, 3-, 4-, and 5-fold GRAPPA, acquisition times were 32, 22, 16, and 12 sec, respectively. In addition to scanning human subjects, we scanned a spherical spectroscopic phantom containing a physiological mixture of metabolite solutions (Cho, Cr, NAA, mI, glutamate, and lactate) with concentrations similar to those found in human brain in vivo. Only fully sampled data were collected for the phantom, using the parameters: TR/TE = 2000/15 ms, matrix size = 32 × 32, FOV = 180 mm, and slice thickness = 15 mm. We performed simulations of parallel imaging by discarding *k*-space data in the K_Y direction, allowing us to investigate SNR degradation in the absence of possible complicating factors such as gradient heating-induced frequency drifts. To compare the SNRs of the 8-channel and 32-channel arrays, we also measured the fully sampled PEPSI data using an 8-channel head array provided by the manufacturer.

GRAPPA Reconstruction and Spectral Postprocessing

Accelerated PEPSI data were reconstructed using a standard GRAPPA algorithm (16). GRAPPA reconstruction is

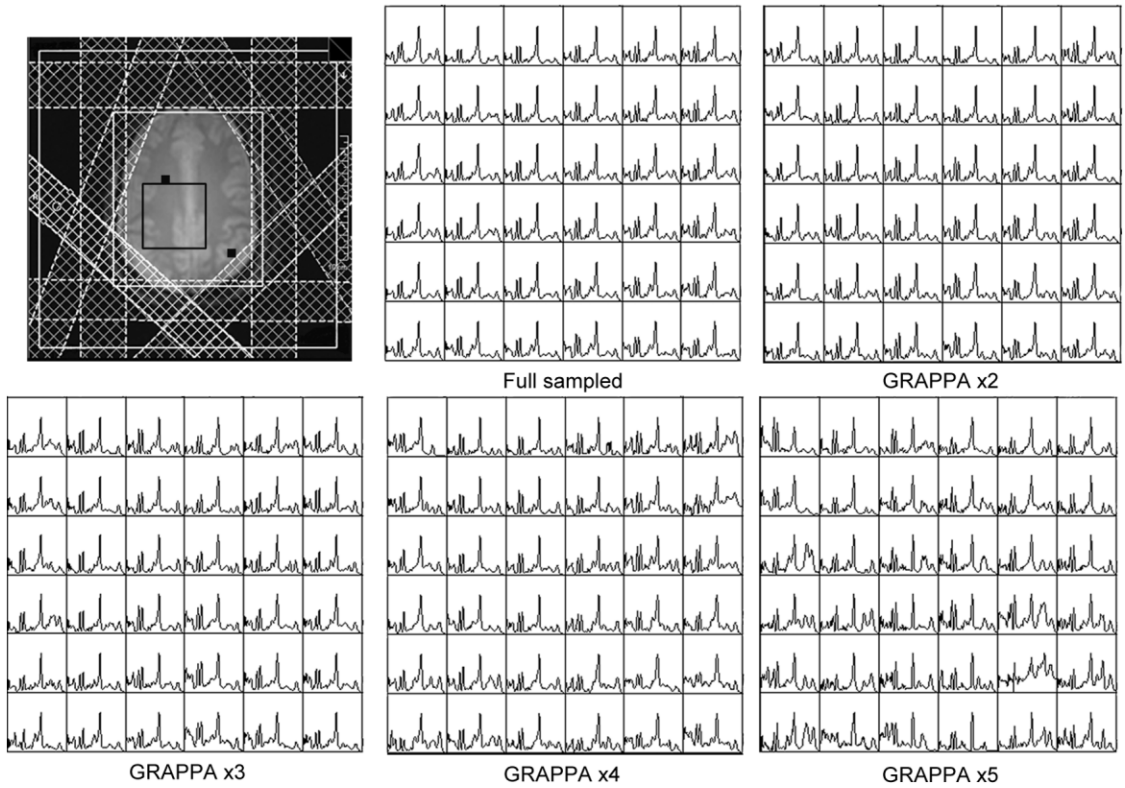

FIG. 1. Localization of the PEPSI experiments and the spatial position for outer volume saturation bands. The central black box indicates the location of the multivoxel spectra. The black squares indicate the locations of voxels for representative spectra shown in Fig. 3. 6 × 6 multivoxel spectra were cut from the fully sampled data and the 2-, 3-, 4-, and 5-fold GRAPPA accelerated data.

based on the generation of spatial harmonics along the acceleration axis K_Y using information from spatially localized coils. We generated uncombined images from each channel of the coil array by applying the reconstruction coefficients to the accelerated data in multiple block-wise reconstructions. The reconstruction coefficients were estimated from the reference data, termed the automatic calibration signal (ACS) lines, which can be acquired from a separate reference scan or from accelerated scans with central *k*-space lines sampled at the Nyquist rate. Because PEPSI requires NWS reference data for automatic phasing, frequency shift, and eddy current corrections, fully sampled NWS reference data were used as the ACS lines in this study. All 32 phase-encoding steps in the NWS image were employed as ACS lines to estimate the reconstruction coefficients; the coefficients were then repetitively applied to reconstruct the entire accelerated WS data using a reconstruction kernel in a 4 by 3 (K_Y by K_X) block. The reconstruction algorithm of SENSE has been described in a previous study (21).

We separately applied automatic zeroth-order spectral phase correction and eddy current correction based on the NWS scan to the GRAPPA-reconstructed even and odd data from the individual coils. We then combined both echoes from each coil channel individually and averaged all channels to produce the spectroscopic images. The phase correction performed before combining data from individual coils was expected to reduce possible artifacts caused by partial phase cancellation and allowed phase-coherent complex data combination (27). In vivo localized spectra were quantified with LCModel-based spectral fitting (28), the range of which was 0.5–4 ppm. LCModel allowed analysis of the in vivo spectra as a linear combination of individual in vitro metabolite spectra, which included simulated macromolecules and lipid components. Metabolite concentrations of NAA, tCr, Cho, mI, and Glu+Gln were obtained using the water-scaling method (28). Metabolite concentration values were computed without partial volume and relaxation correction, and are thus higher than the actual concentration values. All reconstructions were carried out on a regular personal computer in the Matlab programming environment (MathWorks, Natick, MA). The computation time of GRAPPA reconstruction was 10 min for one acceleration rate and spectral fitting can be finished in 2 min.

Spectral and Error Analysis

For the in vitro phantom experiments, the SNR of the NAA peak was evaluated by applying the following formula to both the fully sampled and the accelerated data.

$$\mathrm{SNR} = \frac{\dfrac{\sum_{i \in n_{signal}} s_i}{n_{signal}}}{\sqrt{\dfrac{\sum_{j \in n_{noise}} re(s_j)^2}{n_{noise}}}} \qquad [1]$$

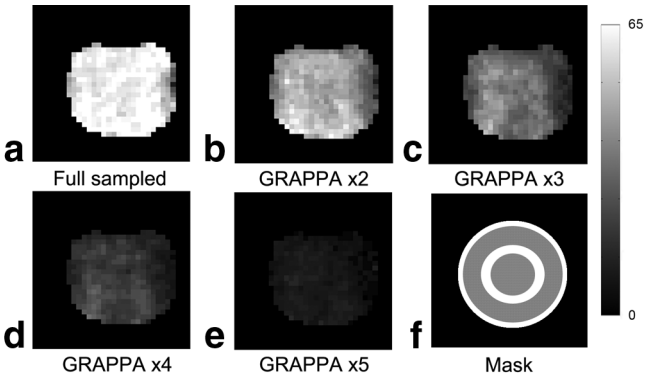

FIG. 2. SNR maps of **(a)** the fully sampled and the **(b)** 2-, **(c)** 3-, **(d)** 4-, and **(e)** 5-fold GRAPPA accelerated data in the phantom experiments. **f:** The shaded areas in the mask depict the ROIs selected from the peripheral and the central regions used in Table 1.

Here, n_{signal} and n_{noise} represent the numbers of spectral points in the metabolite and in the noise ranges, respectively. For the metabolic signals the range was defined in intervals of 0.1 ppm (symmetrical around the peak maximum), whereas the range for noise was from 7.5–8.5 ppm. s*j* indicates the reconstructed spectrum with spectral index *j*. Normalized SNR (nSNR), the ratio between the SNR of GRAPPA-accelerated data and the SNR of fully sampled data listed below, was used to evaluate the reconstruction performance.

$$\text{nSNR} = \frac{SNR_{accelerated}}{SNR_{full\text{-}sampled}} \qquad [2]$$

The SNR and nSNR were calculated at two regions of interest (ROIs) selected from the peripheral and central regions in the phantom, respectively (Fig. 2f).

For in vivo data, the error metric used to quantify metabolite concentration in LCModel was the Cramer–Rao lower bound (CRLB), the lowest bound of the standard deviation (SD) of the estimated metabolite concentration. Expressed in concentration percentage, CRLB can function as an indicator of the reliability for metabolic concentration quantification (28). The CRLB of each metabolite is commonly used to quantify the goodness-of-fit of LCModel (29). Typically, the metabolite concentrations quantified by LCModel with a CRLB of less than 20% are considered acceptable.

Reconstruction errors in the metabolite concentrations were also evaluated in a pixel-by-pixel manner based on the difference in concentrations between the fully sampled and the accelerated data:

$$\text{RMS error (\%)} = \sqrt{\sum_i \left(\frac{C_i^{full} - C_i^R}{C_i^{full}}\right)^2 / N}, \qquad [3]$$

where C^{full} is the concentration from the fully sampled data, C^R is the concentration from the accelerated data after GRAPPA reconstruction, and N is the total number of image voxels in the ROI. The subscript i indicates the spatial location of the image voxel. To present the metabolite maps we used the following thresholds to reject spectroscopic image voxels that could not be fitted with satisfactory accuracy by LCModel: 1) CRLB >50% and 2) spectral linewidth >0.2 ppm. Finally, the metabolite concentration maps were interpolated to a 128 × 128 matrix using zero-filling to improve visualization. To investigate regional differences in the fitting performance, two ROIs, one in the white matter and one in the gray matter, were selected manually on the localization image.

RESULTS

Phantom Experiments

In vitro phantom experiments using the 32-channel array yielded SNR values 3.1- and 2.8-fold greater than those obtained with the 8-channel array in the peripheral region and the central region, respectively (Table 1). Normalized SNR (nSNR) values demonstrated that the soccer ball coil geometry of the 32-channel coil arrays used in our study reduced SNR loss in GRAPPA reconstructions compared with the 8-channel coil array, especially at high acceleration rates. At 4-fold acceleration, nSNR with the 32-channel array was around 0.2 and with the 8-channel array around 0.1 (Table1). We did observe higher SNR at the peripheral region in the fully sampled data and the SNRs generally reduced at higher acceleration rates. SNR became similar in the peripheral and the central regions at acceleration rates over 3 (Table 1). However, the SNR maps did not show spatially related SNR reductions significantly (Fig. 2).

In Vivo Experiments Using the 32-Channel Array Coils

Figure 1 shows the spectra from the 6 × 6 grids at the central region of the brain. The spectra at 2-fold and 3-fold

Table 1
Averaged SNR and Normalized SNR (nSNR) of the Phantom Experiments Measured over Selected ROIs Using a 32-Channel Array and an 8-Channel Array

		Full Sampled	R=2		R=3		R=4		R=5	
		SNR	SNR	nSNR	SNR	nSNR	SNR	nSNR	SNR	NSNR
32 Channel	Peripheral	62.34	41.02	0.66	26.11	0.42	14.61	0.23	6.06	0.10
	Center	57.11	39.97	0.70	25.16	0.44	14.31	0.25	7.71	0.13
8 Channel		20.07	14.11	0.70	7.52	0.37	1.90	0.09		

Compared to the 8-channel array, the 32-channel array offers an approximate SNR gain by a factor of three. We found comparable SNR between 4-fold acceleration using a 32-channel array and 2-fold acceleration using an 8-channel array. The number of voxels in the peripheral and the central ROIs (see Fig. 2) are 165 and 108, respectively.

accelerations were similar in spectral quality to the fully sampled spectra. Noise levels increased noticeably at 4-fold acceleration, but the three major metabolite peaks (NAA, tCr, and Cho) remained clearly detectable. At R = 5 most spectra were contaminated by the enhanced noise levels except several voxels in the central region. Figure 3 shows the reconstructed spectra of two representative voxels located in the white matter (WM) and in the gray matter (GM), displaying the spectral ranges of the metabolites (1–4 ppm) and the noise (6–8 ppm). The noise levels were small at R = 2 and R = 3, indicating that spectra acquired at R = 2 and R = 3 were not significantly different from the fully sampled data. In addition, reconstruction artifacts in these two voxels did not significantly skew the shapes of the baselines. The noise level increased at 4-fold acceleration and the fitting of the three major metabolite peaks (NAA, tCr, and Cho) were affected, which may lead to higher errors in the quantification of metabolite concentrations. At 5-fold acceleration NAA can still be clearly detected, but the further increase in the noise level impaired reliable quantification of the metabolic peaks.

3T in vivo metabolite maps of NAA, tCr, Cho, mI, and Glx with their corresponding CRLB maps are shown in Fig. 4. Whereas NAA, Cho, and mI showed relatively uniform spatial distribution, tCr displayed slight gray-white matter contrast and the Glx maps showed strong gray-white matter contrast. For tCr and Glx, higher concentrations were found in GM than in WM (Table 2), which is consistent with our expectation (30). The concentration ratios between GM and WM (GM/WM) were 1.37 for tCr and 1.67 for Glx, respectively. A comparison between the fully sampled and the GRAPPA-reconstructed data showed that reconstruction artifacts increased noticeably at R = 4 for NAA, tCr, and Cho, but the CRLBs for NAA, tCr, and Cho at this acceleration rate were still lower than 20% (Table 2) for over 95% of the voxels in brain tissue (Fig. 4b). At 5-fold GRAPPA acceleration the concentration maps of NAA, tCr, and Cho showed strong reconstruction artifacts, indicating that such further acceleration failed to preserve the spatial uniformity of the metabolite information. Reconstruction artifacts in the reconstructed mI and Glx metabolite maps increased substantially at 3-fold acceleration (Fig. 4a). As a result, the CRLBs increased significantly (Table 2) and there were over 10% voxels with CRLBs larger than 20% (Fig. 4b). The averaged SNRs for the entire slice were 27.7 for the fully sampled data, 17.7 for R = 2, 11.2 for R = 3, 8.1 for R = 4, and 4.1 for R = 5. The whole-slice-averaged linewidths were around 0.057 ppm for all acceleration rates, but the SDs of the linewidths were 0.015 ppm for the fully sampled data, 0.017 for R = 2, 0.017 for R = 3, 0.018 for R = 4, and 0.024 for R = 5.

There was no significant difference in the CRLBs between GM and WM except for Glx. The CRLBs of Glx were higher in WM than in GM (Table 2), in accordance with the regional concentration difference. The root-mean-square (RMS) errors between the GRAPPA-reconstructed and the fully sampled data are summarized in Table 2. RMS errors were similar between GM and WM for all metabolites except for Glx, which showed higher errors in WM than in GM (Table 2). In general, both RMS errors and CRLBs increased with the acceleration rate. The whole-slice-averaged RMS errors were 18.65%, 17.9%, and 27.84% for NAA, tCr, and Cho at R = 4. For mI and Glx those at R = 2 were 18.65% and 23.98%, respectively.

In Vivo Experiments Using the 8-Channel Array Coils

SENSE and GRAPPA reconstructions showed similar spatial uniformity (Fig. 5). The whole-slice-averaged CRLBs

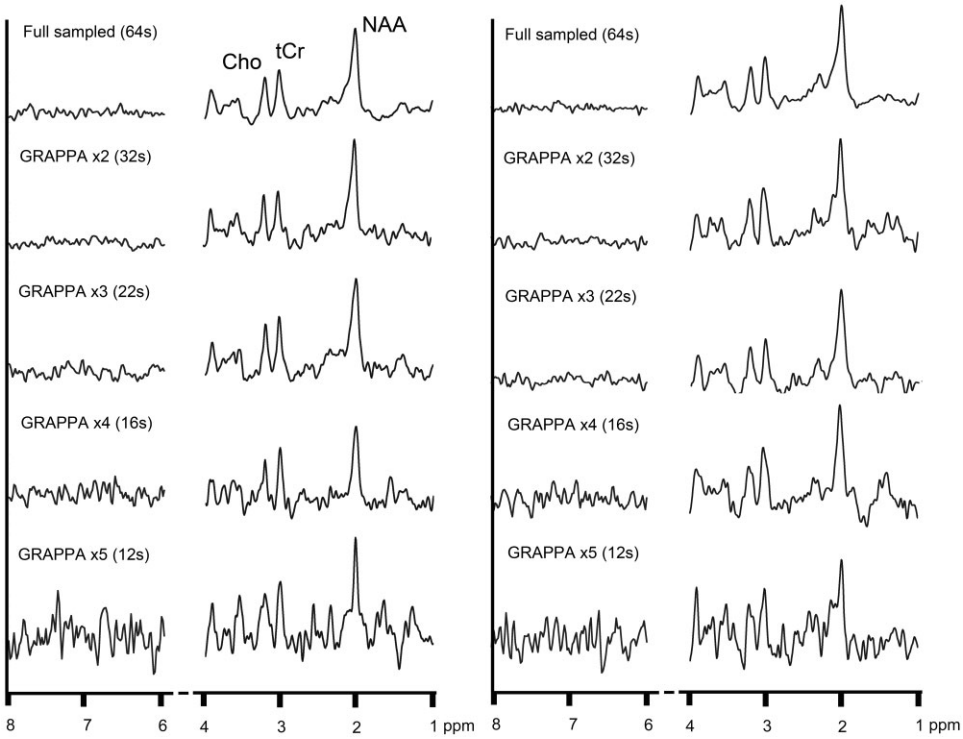

FIG. 3. Two representative spectra from the fully sampled data and the 2-, 3-, 4-, and 5-fold GRAPPA accelerated data (top to bottom). Spectra were selected from the voxels in the white matter at the right hemisphere (left) and in the gray matter at the left lateral area (right), as indicated in Fig. 1. For each spectrum we show the spectral ranges of the metabolites (1–4 ppm) and the noise (6–8 ppm).

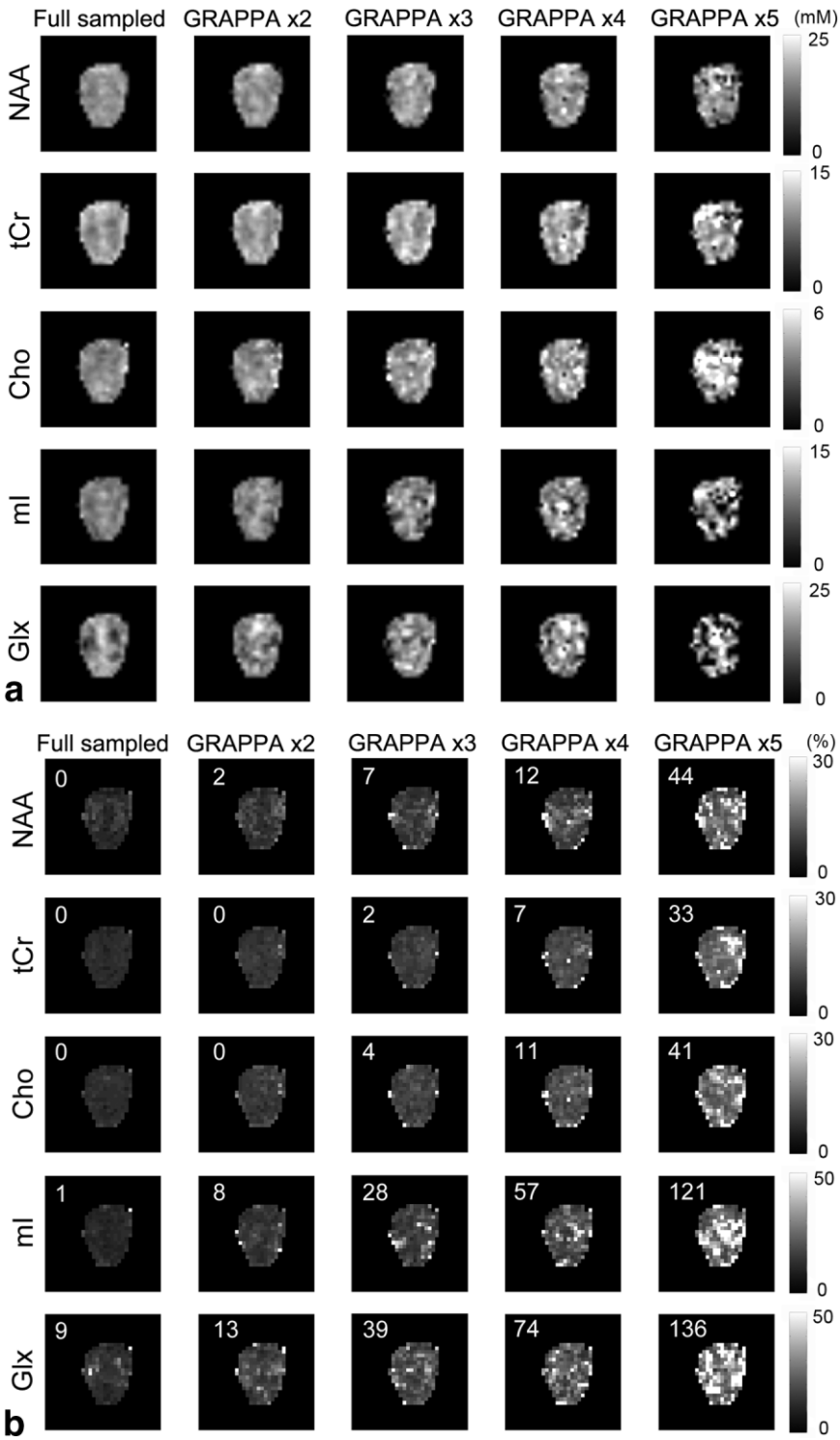

FIG. 4. Metabolite concentration maps **(a)** and CRLB maps **(b)** for NAA, tCr, and Cho in vivo from the fully sampled PEPSI data and the 2-, 3-, 4-, and 5-fold GRAPPA accelerated data. The concentrations were quantified by LCModel. Values shown at the upper left corner of each CRLB map denote the number of voxels with CRLBs over 20%.

(±SD) at R = 2 were 9.7 (±4.11)% for NAA, 8.4 (±2.62)% for tCr, 9.4 (±2.42)% for Cho in GRAPPA, and 8.2 (±3.3)% for NAA, 7.5 (±3.2)% for tCr, 7.9 (±4.5)% for Cho in SENSE. GRAPPA seemed to have higher averaged CRLBs than SENSE but overall the CRLBs were still in an acceptable range (<20%). The concentration difference between SENSE and GRAPPA reconstructions was not statistically significant for any of the metabolites ($P > 0.1$) (Fig. 6). Metabolite maps from SENSE and GRAPPA reconstructions were quantitatively similar. Averaged RMS errors over ROIs defined in GM, WM, and across the whole slice are summarized in Fig. 6. No significant difference in RMS errors was found between the data reconstructed by SENSE and GRAPPA. RMS errors were higher in WM than in GM at 3-fold acceleration except for Cho using GRAPPA reconstruction, which was consistent with the increased reconstruction artifacts and the CRLBs found in WM versus those found in GM (Fig. 5).

Table 2
Average and Standard Deviations of LCModel-Quantified Metabolite Concentrations (mM)

Conc. (mM)		R=1	R=2	R=3	R=4	R=5
WM	NAA	14.46 ± 1.79	15.30 ± 1.77	15.46 ± 2.17	15.36 ± 2.73	15.61 ± 5.77
	tCr	8.71 ± 0.98	9.16 ± 1.02	10.25 ± 2.17	9.43 ± 2.38	9.82 ± 4.15
	Cho	3.19 ± 0.45	3.60 ± 0.63	3.74 ± 0.72	3.85 ± 1.33	5.25 ± 2.90
	mI	6.08 ± 0.83	6.57 ± 1.51	6.53 ± 2.29	6.14 ± 2.63	5.98 ± 3.56
	Glx	11.01 ± 3.20	12.47 ± 4.01	12.91 ± 4.48	13.49 ± 5.69	13.60 ± 10.48
GM	NAA	15.36 ± 2.62	15.93 ± 3.27	15.93 ± 3.12	16.63 ± 4.49	14.38 ± 6.96
	tCr	11.97 ± 1.67	11.93 ± 2.28	11.94 ± 2.35	11.76 ± 3.48	12.13 ± 5.48
	Cho	3.19 ± 0.56	3.10 ± 0.81	3.33 ± 0.80	3.59 ± 1.43	3.79 ± 1.78
	mI	6.11 ± 1.14	6.71 ± 1.47	6.42 ± 2.11	7.42 ± 3.22	8.03 ± 4.05
	Glx	18.40 ± 3.19	17.38 ± 4.76	17.49 ± 5.11	19.06 ± 8.97	14.15 ± 9.36
CRLB (%)		R=1	R=2	R=3	R=4	R=5
WM	NAA	6.58 ± 1.83	7.05 ± 1.90	7.98 ± 2.15	10.65 ± 3.27	17.23 ± 12.01
	tCr	5.23 ± 0.72	6.72 ± 0.73	7.51 ± 1.30	9.77 ± 1.97	16.79 ± 10.48
	Cho	5.16 ± 0.75	6.33 ± 0.81	7.35 ± 1.15	9.67 ± 1.81	13.93 ± 8.40
	mI	7.47 ± 1.18	10.98 ± 2.61	15.21 ± 6.36	24.33 ± 18.50	40.34 ± 37.10
	Glx	12.58 ± 5.20	14.74 ± 4.12	17.88 ± 8.16	23.62 ± 11.00	68.13 ± 74.26
GM	NAA	4.37 ± 1.40	5.77 ± 2.34	6.14 ± 1.78	8.11 ± 5.14	17.43 ± 28.78
	tCr	4.51 ± 0.85	5.86 ± 1.26	6.71 ± 1.18	8.83 ± 4.44	13.24 ± 7.80
	Cho	5.20 ± 0.80	7.20 ± 1.80	8.20 ± 2.36	9.97 ± 3.75	17.62 ± 19.84
	mI	7.69 ± 2.00	10.71 ± 3.48	14.71 ± 10.74	16.29 ± 15.76	25.91 ± 21.60
	Glx	8.00 ± 1.78	12.86 ± 6.50	15.89 ± 6.15	22.03 ± 16.56	51.42 ± 69.23
RMS Error (%)		R=1	R=2	R=3	R=4	R=5
WM	NAA	N/A	11.86	11.90	14.61	26.89
	tCr	N/A	10.27	16.15	18.28	32.38
	Cho	N/A	15.99	17.56	27.26	45.06
	mI	N/A	17.58	26.37	28.80	37.10
	Glx	N/A	27.92	34.55	43.37	63.57
GM	NAA	N/A	10.37	13.82	18.95	23.95
	tCr	N/A	11.61	12.19	17.29	27.46
	Cho	N/A	16.15	20.74	27.50	41.09
	mI	N/A	18.19	24.63	37.89	46.27
	Glx	N/A	16.76	18.30	32.01	35.06

Fitting errors (CRLB in %) and root-mean-square (RMS) errors in metabolite concentrations (%) of NAA, total creatine (tCR), choline (Cho), myo-inositol (mI), and glutamate + glutamine (Glx) in vivo for the fully sampled data and for 2-, 3-, 4-, and 5-fold GRAPPA accelerations. Values were calculated from the ROIs defined in the white matter (WM) and the gray matter (GM) with 60 and 58 voxels, respectively.

DISCUSSION

The results of this study demonstrate the feasibility of combining the GRAPPA parallel MRI technique with PEPSI to further reduce the data acquisition time required for metabolite mapping in the human brain using a 32-channel coil array at 3T. The improved temporal resolution achieved with this approach relies on the intrinsic SNR gains afforded by the smaller RF coil elements in the array and their closer proximity to the head, as well as by the coil geometry, which yields more spatially distinct information from the different channels. In our previous study using an 8-channel coil array at 3T we found that only 2-fold acceleration with 32 sec of measurement time was feasible for maintaining acceptable spectral quality (21). Our present results show that the mean CRLBs were less than 11% for NAA, tCr, and Cho at 4-fold acceleration at 3T with the use of a 32-channel array, such that the scan time for a single signal-averaged short TE PEPSI experiment with the 32 × 32 image matrix, 24 cm FOV, 1.9 cm^3 voxel size can be reduced from 64 sec to 16 sec. Such a reduction in the data acquisition time may enable novel MRSI applications. For example, highly accelerated MRSI can be used in hyperpolarized ^{13}C experiments for its transiently high SNR (31). In addition to improving temporal resolution, partial parallel imaging combined with MRSI is particularly effective for reducing the long scanning time for 3D spatial encoding. As demonstrated here, 1D acceleration by GRAPPA can be utilized to accelerate slow spatial phase encoding in a 2D PEPSI experiment. Further accelerations can be achieved with 2D GRAPPA acceleration in 3D PEPSI experiments in two orthogonal spatial phase-encoding directions. In fact, the spherically symmetric layout of this 32-channel head RF array coil design encourages the use of 2D acceleration.

Here, the achievable GRAPPA acceleration rate was evaluated qualitatively by the spatial variability (homogeneity) in the metabolite maps, and quantitatively by the CRLB and RMS errors in the metabolite concentrations estimated by LCModel. In general, the CRLB from LCModel indicates spectral quality that combines information about SNR, spectral line width, and spectral line shape (28). With our short TE imaging protocol using 1.9 cm^3 nominal spatial resolution (2.1 Hz in spectral resolution and TR/TE of 2000/15 ms), the mean CRLBs are

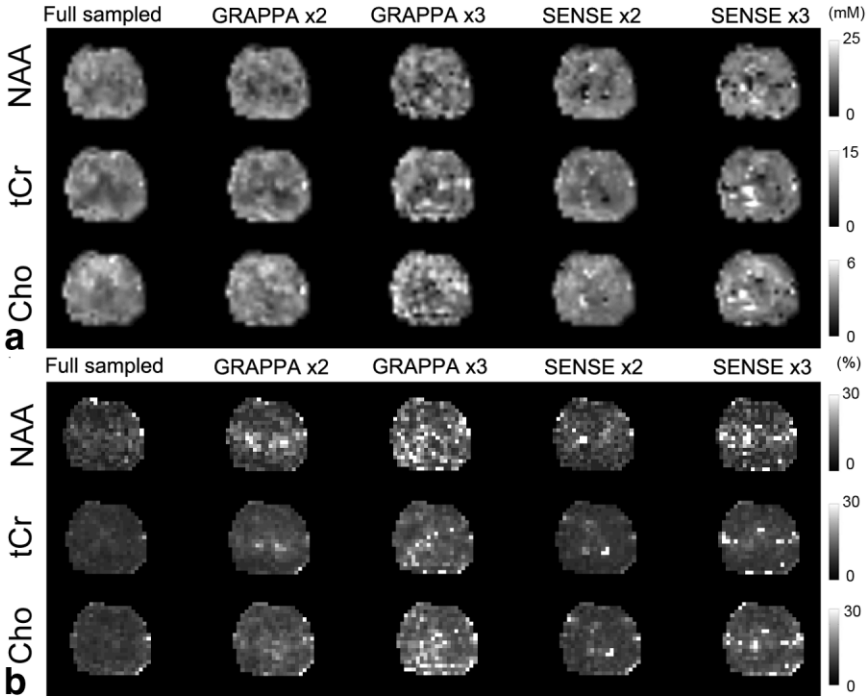

FIG. 5. Metabolite concentration maps **(a)** and CRLB maps **(b)** for NAA, tCr, and Cho from data acquired with an 8-channel phase array coil on another subject. GRAPPA and SENSE reconstructions were performed for 2- and 3-fold accelerated data.

less than 20% and RMS errors are less than 30% for NAA, tCr, and Cho at 4-fold acceleration and for mI and Glx at 2-fold acceleration. However, the maximal acceleration rate should be adjusted to obtain the SNR required for a particular MRSI experiment. It should be noted that the CRLB decreases as SNR increases but the CRLB increase is not expected to be linearly proportional to the SNR reduction (32).

We did not find significant spatial dependence in SNR reductions in the phantom experiments and in the in vivo experiments. For Glx there are significantly higher RMS errors and CRLBs in WM than in GM. Since the fitting of Glx is known to be very sensitive to the noise level, this result can be explained by the lower concentrations of Glx in WM. This finding is also consistent with the higher intrasubject variations of Glx concentrations in WM (28%). For the other metabolites quantified here the intrasubject variations are less than 20% for all other metabolites, which is consistent with values reported in our previous study (30).

Two metabolites, tCr and Glx, show strong GM/WM contrast, which is consistent with the findings from previous reports (30,33). The GM/WM ratios in our study are in the reasonable ranges, although a little lower than the reported values (1.6 ± 0.2 for tCr and 1.8 ± 0.4 for Glx) due to lack of partial volume correction. The concentration values derived here are higher than those reported in previous studies (34,35) due to the lack of partial volume and

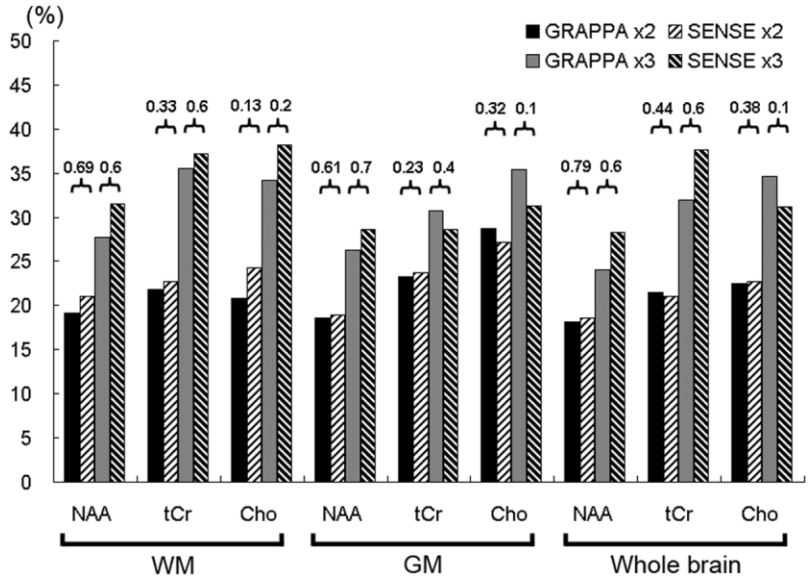

FIG. 6. RMS errors of NAA, tCr, and Cho concentration values from the data acquired with an 8-channel phase array coil. The RMS values are the averages over ROIs defined in WM (66 voxels), in GM (71 voxels), and across the whole slice of the metabolite maps shown in Fig. 5. The numbers in brackets are *P*-values for the statistical significance of differences in concentrations between SENSE and GRAPPA.

Table 3
Comparison of Intersubject Variations (%) of the Metabolite Concentrations between Different Studies

Study	Method	*N*	NAA	tCr	Cho	mI	Glx
Schubert et al. (36)	SVS	40	7.4 %	6 %	11.1 %		
Hurd et al. (37)	SVS	6	6.4 %	10 %	7.1 %		
Posse et al. (30)	PEPSI	9	8.9 %	9.5 %	14.3 %	13.2 %	13.7 %
Present study	PEPSI	5	9.2 %	11.7 %	13 %	14.6 %	9.5 %

N denotes the number of subjects enrolled in the study.

relaxation corrections but in agreement with those measured in our previous works using the 8-channel coil (21). The SDs of the averaged concentrations across subjects are less than 15% for all metabolites. The intersubject coefficients of variations are thus consistent with previous studies (30,36,37) (Table 3). Recently, it has been demonstrated that the PEPSI technique combined with relaxation and partial volume corrections provide metabolic concentrations that are consistent with previous studies (30).

According to our results by comparing the metabolite concentrations, CRLBs, and RMS errors, the difference between GRAPPA and SENSE reconstructions is not statistically significant. The autocalibrating technique is known to help improve the reconstruction of spatial harmonics-based parallel MRI methods such as GRAPPA. In this study we implemented the standard GRAPPA algorithm, where the reconstruction kernel was estimated from the fully sampled NWS data. Because NWS data are acquired for automatic phasing, frequency drift, and eddy current corrections, using the fully sampled NWS PEPSI data as ACS lines is an option that requires no more scanning time than standard PEPSI. Alternatively, a faster reference dataset can be collected using the PEPSI sequence with short TR to complete data acquisition in several seconds. Park et al. (38) recently compared image quality using different reconstruction kernels in GRAPPA reconstruction. They noted that the separation of high-frequency and low-frequency *k*-space ACS lines to estimate the reconstruction kernels improves reconstruction quality. Because the low-frequency *k*-space signals tend to more seriously perturb the reconstruction process, using the same kernel for all *k*-space reconstructions is not optimal. This concept, which implies that GRAPPA PEPSI can be further improved by separating the reconstruction kernels used in the high- and low-frequency regions, is currently being investigated. Our recent results also indicate that GRAPPA calibration is sensitive to the noise amplitude in the ACS lines, which will influence the reconstruction quality of the accelerated PEPSI data (39). On the other hand, an incorporation of prior spectral information may improve GRAPPA reconstruction (40). Because some information, for instance, the spectral pattern, is known before acquisition, it may be possible to further accelerate MRSI by incorporating such prior information for reconstruction (41).

In this study we demonstrated that the SNR improvements associated with the use of a head array with a larger number of small receiver coil elements in a close-fitting helmet design benefit PEPSI spectral quality and acquisition acceleration. The SNR gains observed can also be attributed to the smaller size of the coil elements and their close proximity to the head (25). This SNR improvement is exchanged for a reduction in the acquisition time that can be used for applications for anatomical and functional imaging sequences. Acceleration also reduces motion sensitivity, an improvement desirable for clinical studies. The higher acceleration rate is achievable in part because of this soccer-ball coil geometry, which provides more spatially disparate information from different channels in the array (Table 1). However, simply increasing the number of array channels may not enable further reduction in scanning time. Electromagnetic studies have shown that acceleration beyond 4-fold in one direction at 3T produces dramatic decays in SNR due to fast increases in the geometry factors (42). Nevertheless, the property of increased SNR combined with reduced geometry factors of this 32-channel coil array is still attractive to reduce the lengthy acquisition time of 3D PEPSI using 2D acceleration, which is under development (43). On the other hand, it has been proven that PEPSI provides linear gains in sensitivity with field strengths increased from 1.5T to 7T (44) and enables the mapping of multiplet resonances at high field strength (30). We expect that a short echo time PEPSI technique with large-scale coil array at higher field strength could further improve the performance of parallel PEPSI. However, the technique challenges for short echo time PEPSI at high fields are 1) limitations in the gradient rise times will limit the spectral width at high fields (45), and 2) eddy currents from fast switching of the gradient coils lead to line-shape distortions, particularly at short TE.

In conclusion, combining a 32-channel coil array with GRAPPA reconstruction can improve the temporal resolution of MRSI experiments to reduce encoding time.

ACKNOWLEDGMENT

This work was supported by National Institutes of Health Grants R01 HD040712, R01 NS037462, P41 RR14075, R21 EB007298, National Science Council—Taiwan (NSC 96-2320-B-002-085), National Health Research Institute—Taiwan (E29C97N), and the Mental Illness and Neuroscience Discovery Institute (MIND).

REFERENCES

1. Maudsley AA, Matson GB, Hugg JW, Weiner MW. Reduced phase encoding in spectroscopic imaging. Magn Reson Med 1994;31:645–651.
2. Duyn JH, Moonen CT. Fast proton spectroscopic imaging of human brain using multiple spin-echoes. Magn Reson Med 1993;30:409–414.
3. Dreher W, Leibfritz D. Fast proton spectroscopic imaging with high signal-to-noise ratio: spectroscopic RARE. Magn Reson Med 2002;47:523–528.
4. Ebel A, Dreher W, Leibfritz D. A fast variant of (^{1})H spectroscopic U-FLARE imaging using adjusted chemical shift phase encoding. J Magn Reson 2000;142:241–253.

5. Guimaraes AR, Baker JR, Jenkins BG, Lee PL, Weisskoff RM, Rosen BR, Gonzalez RG. Echoplanar chemical shift imaging. Magn Reson Med 1999;41:877–882.
6. Adalsteinsson E, Irarrazabal P, Topp S, Meyer C, Macovski A, Spielman DM. Volumetric spectroscopic imaging with spiral-based k-space trajectories. Magn Reson Med 1998;39:889–898.
7. Mansfield P. Spatial mapping of the chemical shift in NMR. Magn Reson Med 1984;1:370–386.
8. Posse S, DeCarli C, Le Bihan D. Three-dimensional echo-planar MR spectroscopic imaging at short echo times in the human brain. Radiology 1994;192:733–738.
9. Webb P, Spielman D, Macovski A. A fast spectroscopic imaging method using a blipped phase encode gradient. Magn Reson Med 1989;12:306–315.
10. Posse S, Dager SR, Richards TL, Yuan C, Ogg R, Artru AA, Muller-Gartner HW, Hayes C. In vivo measurement of regional brain metabolic response to hyperventilation using magnetic resonance: proton echo planar spectroscopic imaging (PEPSI). Magn Reson Med 1997;37:858–865.
11. Posse S, Tedeschi G, Risinger R, Ogg R, Le Bihan D. High speed 1H spectroscopic imaging in human brain by echo planar spatial-spectral encoding. Magn Reson Med 1995;33:34–40.
12. Dager SR, Friedman SD, Heide A, Layton ME, Richards T, Artru A, Strauss W, Hayes C, Posse S. Two-dimensional proton echo-planar spectroscopic imaging of brain metabolic changes during lactate-induced panic. Arch Gen Psychiatry 1999;56:70–77.
13. Dager SR, Friedman SD, Parow A, Demopulos C, Stoll AL, Lyoo IK, Dunner DL, Renshaw PF. Brain metabolic alterations in medication-free patients with bipolar disorder. Arch Gen Psychiatry 2004;61:450–458.
14. Sodickson DK, Manning WJ. Simultaneous acquisition of spatial harmonics (SMASH): fast imaging with radiofrequency coil arrays. Magn Reson Med 1997;38:591–603.
15. Pruessmann KP, Weiger M, Scheidegger MB, Boesiger P. SENSE: sensitivity encoding for fast MRI. Magn Reson Med 1999;42:952–962.
16. Griswold MA, Jakob PM, Heidemann RM, Nittka M, Jellus V, Wang J, Kiefer B, Haase A. Generalized autocalibrating partially parallel acquisitions (GRAPPA). Magn Reson Med 2002;47:1202–1210.
17. Sanchez-Gonzalez J, Tsao J, Dydak U, Desco M, Boesiger P, Pruessmann KP. Minimum-norm reconstruction for sensitivity-encoded magnetic resonance spectroscopic imaging. Magn Reson Med 2006;55:287–295.
18. Dydak U, Weiger M, Pruessmann KP, Meier D, Boesiger P. Sensitivity-encoded spectroscopic imaging. Magn Reson Med 2001;46:713–722.
19. Zhao X, Prost RW, Li Z, Li SJ. Reduction of artifacts by optimization of the sensitivity map in sensitivity-encoded spectroscopic imaging. Magn Reson Med 2005;53:30–34.
20. Dydak U, Pruessmann KP, Weiger M, Tsao J, Meier D, Boesiger P. Parallel spectroscopic imaging with spin-echo trains. Magn Reson Med 2003;50:196–200.
21. Lin FH, Tsai SY, Otazo R, Caprihan A, Wald LL, Belliveau JW, Posse S. Sensitivity-encoded (SENSE) proton echo-planar spectroscopic imaging (PEPSI) in the human brain. Magn Reson Med 2007;57:249–257.
22. Serafini S, Steury K, Richards T, Corina D, Abbott R, Dager SR, Berninger V. Comparison of fMRI and PEPSI during language processing in children. Magn Reson Med 2001;45:217–225.
23. de Zwart JA, Ledden PJ, van Gelderen P, Bodurka J, Chu R, Duyn JH. Signal-to-noise ratio and parallel imaging performance of a 16-channel receive-only brain coil array at 3.0 Tesla. Magn Reson Med 2004;51:22–26.
24. Hardy CJ, Cline HE, Giaquinto RO, Niendorf T, Grant AK, Sodickson DK. 32-element receiver-coil array for cardiac imaging. Magn Reson Med 2006;55:1142–1149.
25. Wiggins GC, Triantafyllou C, Potthast A, Reykowski A, Nittka M, Wald LL. 32-Channel 3 Tesla receive-only phased-array head coil with soccer-ball element geometry. Magn Reson Med 2006;56:216–223.
26. Blaimer M, Breuer F, Mueller M, Heidemann RM, Griswold MA, Jakob PM. SMASH, SENSE, PILS, GRAPPA: how to choose the optimal method. Top Magn Reson Imaging 2004;15:223–236.
27. Zhu X, Ebel A, Ji JX, Schuff N. Spectral phase-corrected GRAPPA reconstruction of three-dimensional echo-planar spectroscopic imaging (3D-EPSI). Magn Reson Med 2007;57:815–820.
28. Provencher SW. Estimation of metabolite concentrations from localized in vivo proton NMR spectra. Magn Reson Med 1993;30:672–679.
29. Srinivasan R, Sailasuta N, Hurd R, Nelson S, Pelletier D. Evidence of elevated glutamate in multiple sclerosis using magnetic resonance spectroscopy at 3 T. Brain 2005;128(Pt 5):1016–1025.
30. Posse S, Otazo R, Caprihan A, Bustillo J, Chen H, Henry PG, Marjanska M, Gasparovic C, Zuo C, Magnotta V, Mueller B, Mullins P, Renshaw P, Ugurbil K, Lim KO, Alger JR. Proton echo-planar spectroscopic imaging of J-coupled resonances in human brain at 3 and 4 Tesla. Magn Reson Med 2007;58:236–244.
31. Golman K, Ardenkjaer-Larsen JH, Petersson JS, Mansson S, Leunbach I. Molecular imaging with endogenous substances. Proc Natl Acad Sci U S A 2003;100:10435–10439.
32. Kreis R. Issues of spectral quality in clinical 1H-magnetic resonance spectroscopy and a gallery of artifacts. NMR Biomed 2004;17:361–381.
33. Srinivasan R, Cunningham C, Chen A, Vigneron D, Hurd R, Nelson S, Pelletier D. TE-averaged two-dimensional proton spectroscopic imaging of glutamate at 3 T. Neuroimage 2006;30:1171–1178.
34. Gasparovic C, Song T, Devier D, Bockholt HJ, Caprihan A, Mullins PG, Posse S, Jung RE, Morrison LA. Use of tissue water as a concentration reference for proton spectroscopic imaging. Magn Reson Med 2006;55:1219–1226.
35. Soher BJ, Hurd RE, Sailasuta N, Barker PB. Quantitation of automated single-voxel proton MRS using cerebral water as an internal reference. Magn Reson Med 1996;36:335–339.
36. Schubert F, Gallinat J, Seifert F, Rinneberg H. Glutamate concentrations in human brain using single voxel proton magnetic resonance spectroscopy at 3 Tesla. Neuroimage 2004;21:1762–1771.
37. Hurd R, Sailasuta N, Srinivasan R, Vigneron DB, Pelletier D, Nelson SJ. Measurement of brain glutamate using TE-averaged PRESS at 3T. Magn Reson Med 2004;51:435–440.
38. Park J, Zhang Q, Jellus V, Simonetti O, Li D. Artifact and noise suppression in GRAPPA imaging using improved k-space coil calibration and variable density sampling. Magn Reson Med 2005;53:186–193.
39. Rueckert M, Otazo R, Posse S. GRAPPA reconstruction of sensitivity encoded 2D and 3D proton echo planar spectroscopic imaging (PEPSI) with SNR adaptive recalibrating. In: Proc 14th Annual Meeting ISMRM, Seattle; 2006. p 296.
40. Lin FH. Prior-regularized GRAPPA reconstruction. In: Proc 14th Annual Meeting ISMRM, Seattle; 2006. p 3656.
41. Lin FH, Kwong KK, Belliveau JW, Wald LL. Parallel imaging reconstruction using automatic regularization. Magn Reson Med 2004;51:559–567.
42. Wiesinger F, Boesiger P, Pruessmann KP. Electrodynamics and ultimate SNR in parallel MR imaging. Magn Reson Med 2004;52:376–390.
43. Otazo R, Tsai SY, Lin FH, Posse S. Accelerated short-TE 3D proton echo-planar spectroscopic imaging using 2D-SENSE with a 32-channel array coil. Magn Reson Med 2007;58:1107–1116.
44. Otazo R, Mueller B, Ugurbil K, Wald L, Posse S. Signal-to-noise ratio and spectral linewidth improvements between 1.5 and 7 Tesla in proton echo-planar spectroscopic imaging. Magn Reson Med 2006;56:1200–1210.
45. Ebel A, Maudsley AA, Weiner MW, Schuff N. Achieving sufficient spectral bandwidth for volumetric 1H echo-planar spectroscopic imaging at 4 Tesla. Magn Reson Med 2005;54:697–701.